RSC Advances

ROYAL SOCIETY OF CHEMISTRY

www.rsc.org/advances

Highly sensitive and selective ethanol and acetone gas sensors by adding some dopants (Mn, Fe, Co, Ni) on hexagonal ZnO plates.

Mohammad Hossein Darvishnejad[a], Azam Anaraki Firooz[a,*], Javad Beheshtian[a,*], Abbas Ali Khodadadi[b]

Abstract

1 mol% of Mn-, Fe-,Co- and Ni -doped and single phase hexagonal ZnO plates have been synthesized by a simple low temperature hydrothermal method using D-ribose as a template. The influence of the doped species on structural, optical and sensing property was studied by X-ray diffraction (XRD), scanning electron microscopy (SEM), UV–Vis spectra, photoluminescence (PL) and gas sensor characterization system. The results show that the doped species have significant effect on morphology, crystallite size, photoluminescence and sensing properties. Co-doped ZnO shows the highest response of 570 and selectivity to 300 ppm ethanol than the other sensors. In addition, Mn- and Ni-doped ZnO sensors show selective response to acetone in presence of CO and ethanol. While, Fe-doped ZnO shows no considerable response to CO, ethanol and acetone gases.

[a] Department of Chemistry, Faculty of Science, Shahid Rajaee Teacher Training University, P.O. Box 167855-163 Tehran, Iran. Corresponding author: E-mail: a.anaraki@srttu.edu (A. Anaraki Firooz), Co corresponding author: E-mail: j.beheshtian@gmail.com (J. Beheshtian)

[b]Oil & Gas Processing Center of Excellence, School of Chemical Engineering, University of Tehran, 11155-4563 Tehran, Iran

1. Introduction

Many industrial and commercial activities involve the monitoring and control of the environment, with application sighting from domestic gas alarms and medical diagnostic system to safety, environmental and chemical plant instrumentation. The largest barrier to achieve improved process or environmental control often lies at the interface between the system and the environment to be monitored, i.e. the sensor. Without sensors, significant advances in control and instrumentation will not be possible.[1] Semiconductor sensors detect gases by a chemical reaction that takes place when the gas comes in direct contact with the sensor. Among these semiconductors, zinc oxide is an interesting compound with a wide bandgap of ~3.37 eV, which is suitable in many fields, such as solar cells, piezoelectric devices, electromagnetic shielding and gas sensors.[2] ZnO, as one of the most important materials for gas sensor, has already shown good response to pollutant gases such as H_2S, SO_2, CO_2, and benzene [3,4] , and explosive gases such as H_2,CH_4, CO, ethanol and acetone. [5–7] In addition, doping of ZnO with different elements, such as noble metals, transition metals, or metal oxides, has been reported to be a beneficial access to ameliorate the electrical conductivity when they are used in gas sensing devices. For examples, Navale et. al observed that undoped ZnO responses tangibly to LPG while Ru doped ZnO sample highly senses ethanol vapors.[8] Niu et. al used Fe, Co, and Cr as dopants to improve the gas sensing property of pure ZnO,and the results demonstrated that $ZnFe_2O_4$ had high sensitivity and good selectivity to Cl_2. [9] Zhang et. al found that the TiO_2-doped ZnO sensor exhibited remarkably enhanced response to 100 ppm toluene even at a lower temperature of 290°C. [10] Ning et. al found that the Sn and Fe dopants increased gas response of ZnO to formaldehyde at 300°C, while Ti dopant decreased the gas sensing property of ZnO.[11] In this investigation, we studied the doping effect on the morphology, crystal structure, band gap, crystal defect and gas sensing property of ZnO. We used four typical dopants as Mn, Fe, Co and Ni to study their effects on the gas sensor response and selectivity.

2. Experimental

2.1. Preparation of ZnO and Mn-, Fe-, Co -, Ni-doped ZnO

All chemicals were prepared by hydrothermal method and the concentration of dopants was 1.0 mol % (mole ratio of dopant to Zn is 0.01). 5 mmol Zn(Ac)2·2H2O and 10 mmol ribose were dissolved in 50 ml distilled water, were mixed and the stirring was continued for 30 min at room temperature. After stirring, 0.05 mmol Mn or Fe or Co or Ni acetate were added to solution and again stirred for 30 min. After that time, 10 mmol NaOH was added to solution. The achieved solution was then transferred to a

Teflon lined autoclave, and sealed and heated up to 90 ◦C for 2 h. After completion of the reaction, the autoclave was allowed to cool at room temperature followed by washing with water serially and dried at room temperature. The sample after doping with Mn, Fe, Co and Ni which will be named as Mn-ZnO, Fe-ZnO, Co-ZnO and Ni-ZnO, respectively.

2.2. Characterization

The morphology and size of the products were characterized by scanning electron microscopy (SEM Holland Philips XL30).The crystalline phase was determined by powder X-ray diffraction (XRD using λ (Cu Kα) = 1.5418 Å). The PL spectra were recorded at room temperature by a 300 nm excitation from Xe lamp (Avantes/Avaspec 2048). The ultraviolet–visible (UV–vis) absorption spectra were measured on a spectrophotometer (Rayleig).

2.3 Gas sensing measurements

A homogeneous paste of ZnO, Mn-, Fe-, Co- and Ni-doped ZnO is prepared by addition of water. The paste was screen-printed on an alumina substrate, on which gold electrodes were deposited. The sensors were dried and calcined at 400°C for 4 h. Then, the sensors were located in a quartz holder in a furnace, the temperature of which was controlled by a PID temperature controller. The sensor was connected to an electrical circuit using platinum wires. The DC electrical measurement was made using a voltage of 4.0 V applied on a known resistance in series with the sensor.

The DC voltage across the sensor was read out using an A/D converter interfaced to a computer for further processing. The electrical resistance of the sensors was measured in air and in the target gases as ethanol, CO and acetone in the working temperature range from 200°C to 400°C. The gas response was defined by S, as the ratio R_a/R_g, where R_a is the electrical resistance of sensors in air and R_g is their resistance at 300 ppm of CO, ethanol and acetone, at the same temperature. Fig.1 shows the schematic diagram of the gas sensor system.

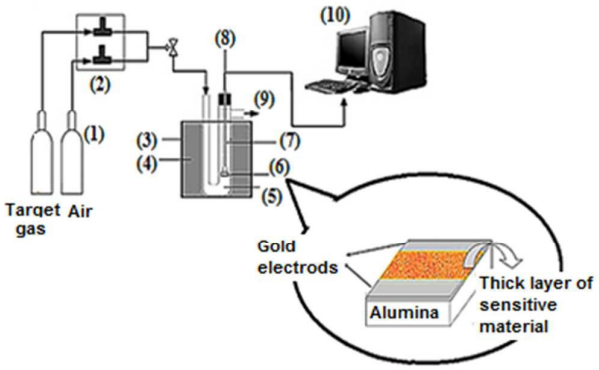

Fig. 1: Schematic diagram of the gas sensor system including: (1) Gas capsules (2) Gas mass flow controller (3) Steel furnace (4) Asbestos (5) Glass reactor (6) Location sensor (schematic diagram of the gas sensor structure) (7) Glass tubes and wires platinum (8)Thermocouple (9) Gas output (10) Computer

3. Results and discussions

3.1. Crystal structure and morphology

X-ray diffraction (XRD) is performed to determine the crystalline structures of the samples. Fig. 2 shows the XRD patterns of the undoped and Mn-, Fe-, Co-, Ni - ZnO. The observed diffraction reflections, i.e. (100), (002), (101), (102), (110), (103), (200), (112) and (201) are similar to bulk ZnO and correspond to wurtzite hexagonal phase of ZnO with standard JCPDS data card No. 36-1451. No reflections characteristic related to Mn, Fe, Co, Ni and other related metal oxides or other crystalline forms is observed in the pattern, indicating that either Mn, Fe, Co or Ni ions replace Zn ions in the lattice of ZnO crystals due to smaller or/ similar ionic radius or formed crystallites are too small to be detected via XRD.[12] Scanning electron microscopy (SEM) is employed to study the morphology of samples. The morphology of undoped and doped ZnO is shown in Fig. 3, which shows all of the samples are hexagonally plate except Ni-ZnO that is rods with hexagonally plate cross sections. Its average height and diameter is 1000 and 400 nm, respectively. Mn-ZnO shows the smallest hexagonally plate with average height and diameter of 100 and 175 nm, respectively (Table 1). The main reason for this different morphology is due to different ionic radius in dopants. Mn^{2+}(0.066) and Fe^{2+} (0.063 nm) have larger radius than Zn^{2+} (0.060 nm), while, Co^{2+}(0.058) and Ni^{2+} (0.055 nm) are smaller.[13] Wu et al.[14] pointed out that dopant atoms had a strong influence on the morphology and the doping process is a kinetic equilibrium process of thermodynamic equilibrium and dynamic equilibrium.

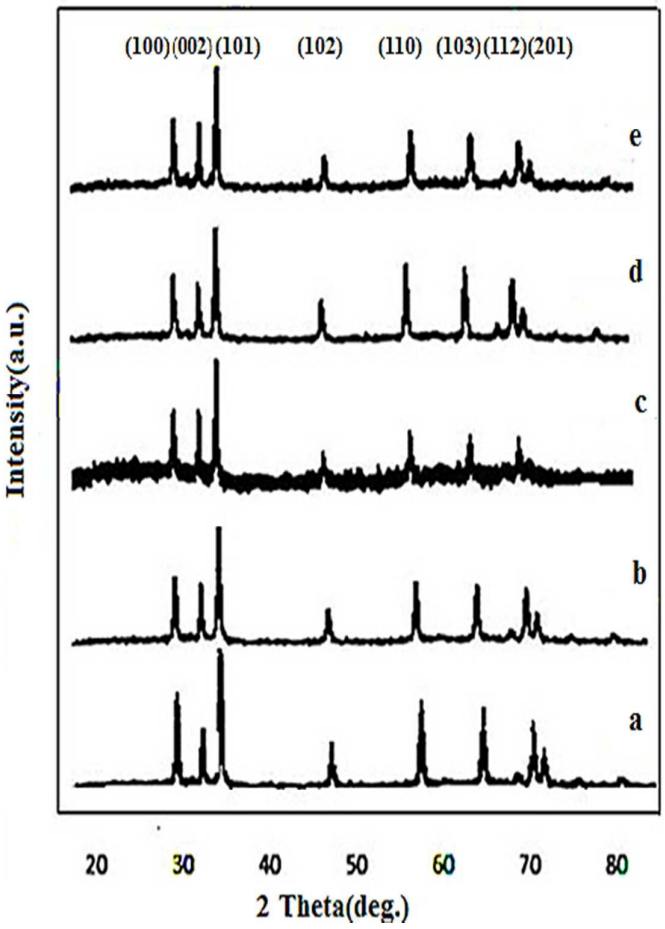

Fig.2. XRD patterns of (a) ZnO, (b) Mn-ZnO (c) Fe-ZnO, (d) Co-ZnO (e) Ni-ZnO samples.

Table.1. Morphologies, diameters size and Band gaps of the ZnO and doped ZnO nanostructured samples.

Sample	Morphology	Average Height and diameter of hexagonal plate (nm)	Bandgap (eV) (Experimental)
ZnO	Hexagonal plates	175-1000	3.27
Mn-ZnO	Hexagonal plates	75- 100	3.24
Fe-ZnO	Hexagonal plates	150-250	3.21
Co-ZnO	Hexagonal plates	150-600	3.24
Ni-ZnO	Nanoroods with hexagonal plates cross sections	1000- 400	3.26

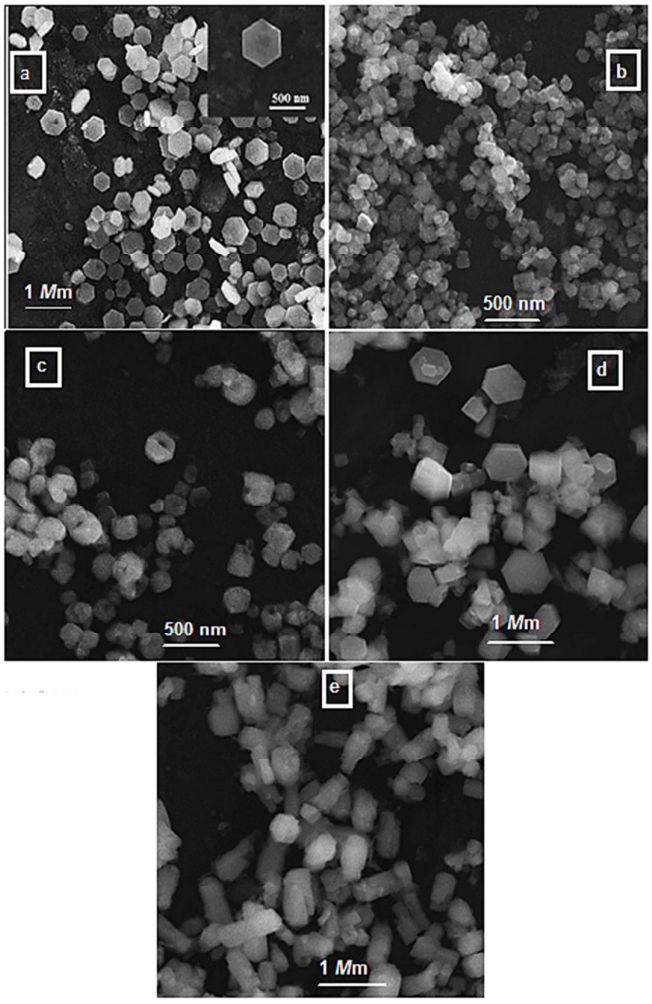

Fig.3. SEM images of (a) ZnO, (b) Mn-ZnO (c) Fe-ZnO, (d) Co-ZnO (e) Ni-ZnO samples.

On the other hand, the incorporation of dopant into the host is hindered through an increase of surface energy and lattice distortion. In particular, the thermodynamically unfavored, purely kinetically driven growth of one dimensional structure is often restrained.[15] Moreover, Zn^{2+} is tetrahedrally coordinated with four O^{2-}, and these ions are systematically substituted into Zn^{2+} ions sites within the ZnO crystal lattice with the same coordination without changing the wurtzite structure of the parent ZnO and it is in good agreement with the earlier reports.[11] However, when Zn^{2+} is substituted with Ni, the morphology becomes rod with a hexagonal cross section. It means that Ni doping may decrease the nucleation rate of Ni-ZnO and hydrothermal production, helpful for the regular growths of the Ni-ZnO nanorods. According to previous paper it is reasonable to suggest that Ni doping favor the growth of ZnO rods .[14]

3.2. UV–Vis absorption and PL spectra

It is well known that dopant can affect crystal defect and band gap of semiconductor.[16] Thus, we studied the band gap of undoped and doped ZnO by UV–Vis reflectance and absorption spectra. Fig. 4 shows the observed UV-Vis absorption spectra of the samples. Summarized in Table 1, the band gaps of the samples are calculated based on the maximum absorption waves and according to Kubelka-Munk equation: $\alpha = K(h\nu - E_g)^{(1/n)}/h\nu$, where α is the absorption coefficient, E_g is the band-gap energy (eV), K is

a constant, n equals 0.5 for indirect transition and 2 for the direct transition and ZnO is considered as an direct semiconductor. The band-gaps of doped ZnO samples are smaller than that of undoped ZnO. The smallest band gap is for Fe- ZnO.

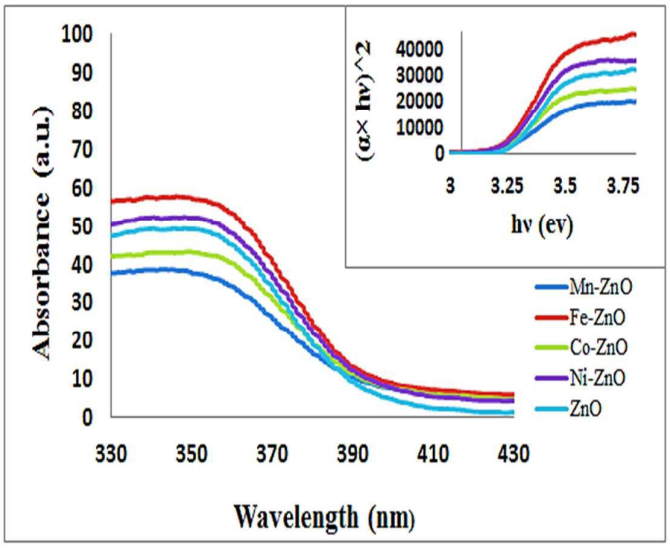

Fig.4. UV–vis adsorption and reflectance spectra of the ZnO and doped ZnO nanostructur samples.

The experimental band-gap energy of the undoped ZnO which is around 3.27 eV was adopted as the benchmark to correct the calculated values of ZnO band gap.

Photoluminescence (PL) spectroscopy is a significant instrument to characterize the intrinsic and extrinsic defects in semiconductors. Figs.5 and 6 show the PL spectra of all the samples using an excited wavelength of 300 and 400 nm, respectively. As shown in Fig. 5, there is a peak in the range of 380-390 nm in all samples that is attributed to the band edge excitonic luminescence of ZnO and doped ZnO. The defects could affect the position of the band-edge emission as well as the shape of the luminescence spectrum.[17] For all samples, except Fe- and Ni- ZnO, there are two blue emission bands in the range of 420-425 and 488 nm. In addition, there is another blue emission band in the range of 445-450 nm for all samples.

The blue emission in the range of 420-425 is usually attributed to the near band edge (NBE) emission due to free exciton recombination[18]. The emission about 488 nm is related to deep level emissions (DLE). This emission in ZnO has been frequently ascribed to several intrinsic and extrinsic defects that are due to electron recombination in oxygen vacancy with a hole in the valence band [19].

The peaks at 445-450 nm are attributed to different defects associated with the host lattice.

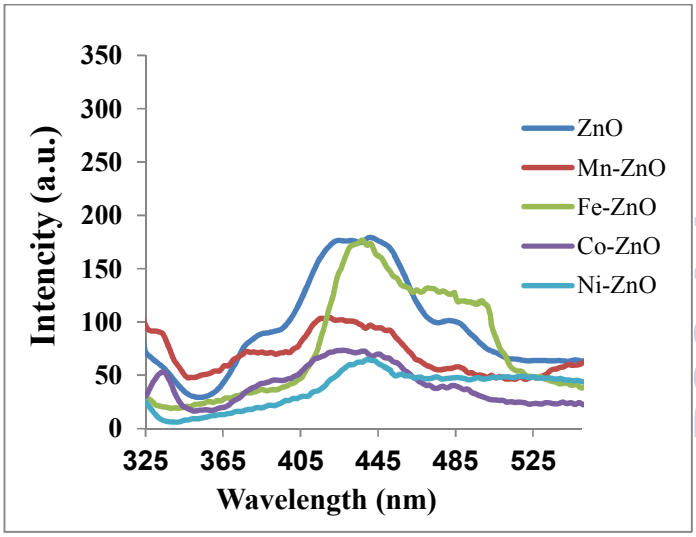

Fig.5. PL spectra of the ZnO and doped ZnO samples using an excited wavelength of 300 nm.

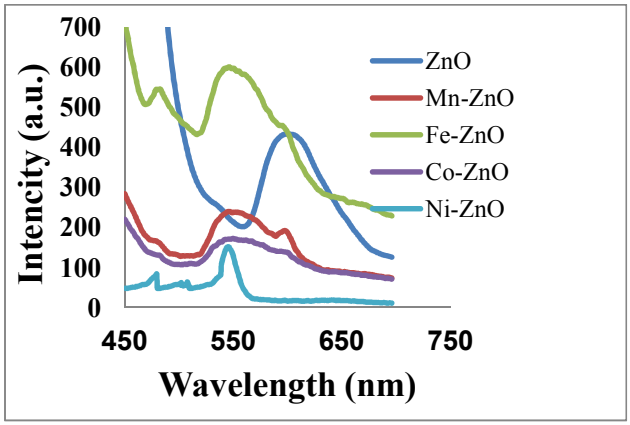

Fig. 6: PL spectra of the ZnO and doped ZnO samples using an excited wavelength of 400 nm.

As shown in Fig. 6, there are two green emission bands in the range of 530 and 590 nm. These bands are related to oxygen vacancies.

3.3 Gas sensing properties

3.3.1 Working Temperature

Sensor response of undoped and doped-ZnO towards CO, C_2H_5OH and CH_3COCH_3 is investigated at various temperatures. The sensor response (S) is defined as $S = R_{air}/R_{gas}$, where R_{air} and R_{gas} are resistances of sensors in presence of air and the target gas, respectively. Fig. 7 shows the sensor responses (S) to the gases measured in the temperature range of 200°C to 400°C.

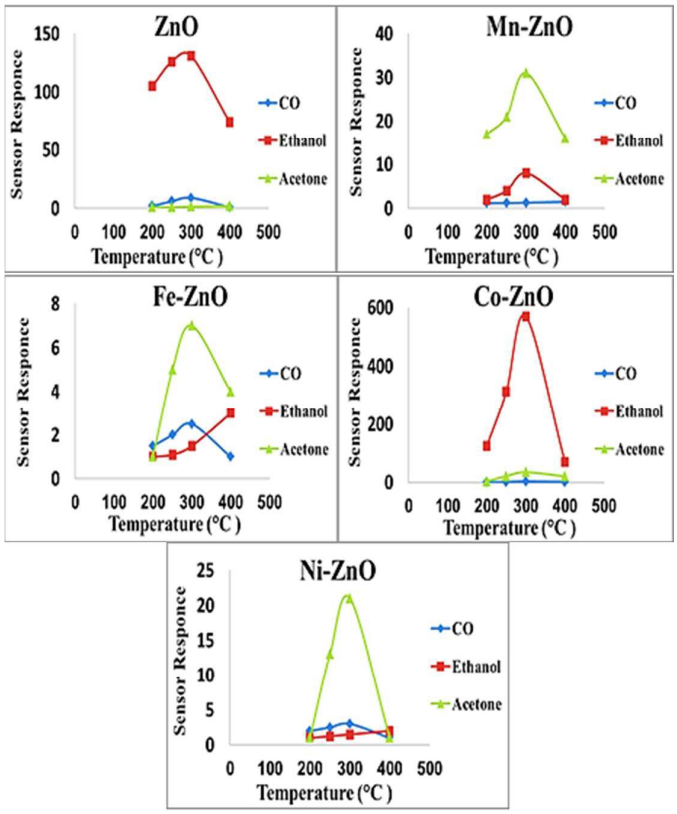

Fig.7. Response of ZnO and doped ZnO nanostructure sensors as a function of operating temperature to 300 ppm CO, ethanol and acetone.

All the sensors exhibit maximum responses to CO, ethanol and acetone at 300°C. On the other hand the responses increase and reach their maximums at 300°C, and then decreased rapidly with increasing the temperature. According to paper [20], this tendency resulted from the competition between slow kinetics at low temperatures and enhanced desorption at high temperatures.

Further, the increase in response with increasing working temperature can be explained by adsorption and desorption of oxygen. With

increasing testing temperature the response increases for the sensors based on ZnO due to increasing the number of surface electron. It causes to dissociate and adsorb higher amount of oxygen molecule on the active sites. As a result, depletion layer forms and resistance increases. When the number of adsorption of oxygen molecules increase, the number of electron withdrawal from ZnO will increase and thus depletion layer formation will be larger. When reducing gases react with this adsorbed oxygen the change in resistance is higher which leads into improvement of response. Therefore, response increases with increasing temperature.[21]

3.3.2 Sensor response and selectivity

Gas sensors for practical applications are required to have very good sensor response and selectivity to the targeted molecules. Three typical gases (ethanol, acetone and CO) were selected as target gases to investigate the gas response at operating temperature of 200-400°C. The undoped ZnO and Co- ZnO gas sensors (Fig.7) show good selectivity to ethanol, while, Mn- and Ni- ZnO gas sensors show good selectivity to acetone gas. The maximum response of Co- ZnO sensor to ethanol is 570 at 300^{o}C, whereas this sensor shows a little response to CO and acetone.

This sensor shows the highest response to ethanol compared with the other sensors. The response of this gas sensor to ethanol is more than 4 times higher than that of the undoped ZnO sensor. The maximum response of Mn- ZnO sensor to acetone is 30 at 300^{o}C, whereas this sensor shows a little response to ethanol and CO. The response of this gas sensor to acetone is about 1.5 times higher than that of Ni- ZnO sensor. In contrast, Fe- ZnO sensor shows no considerable responses to all mentioned gases. Fig.8 shows the variation in sensor response of Mn-ZnO sensor with acetone concentration ranging from 50 ppm to 300 ppm. The sensor response is linear at this range of acetone concentration. When the sensor exposes to 50 ppm acetone the sensor response is ~ 6, and as the acetone concentration is raised to 300 ppm, the sensor response increases nearly linearly up to ~30.

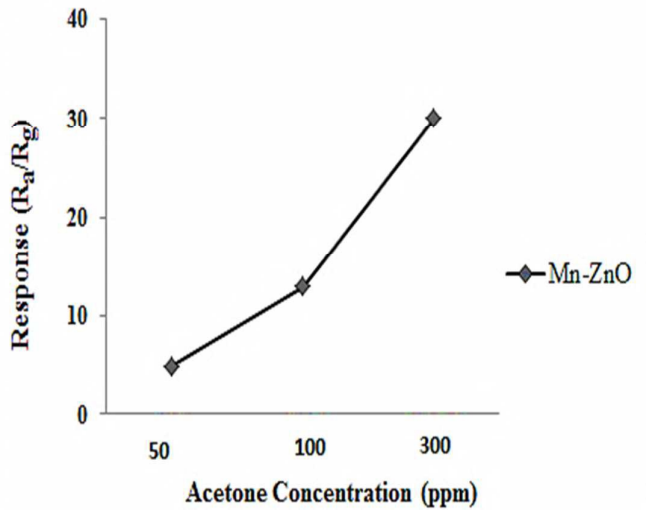

Fig.8. The variation in sensor response of Mn-ZnO sensor with acetone concentration ranging from 50 ppm to 300ppm.

3.3.3 Response-recovery characteristic

Response and recovery times are defined as the time required after switching from air to gas and vice versa to reach the 90% response and returning to original resistance, respectively. Table 2 shows the response and recovery times of some sensors such as undoped ZnO, Co-, and Mn- ZnO sensors. These selected Co-and Mn-ZnO sensors show the highest selectivity to ethanol and acetone gas, respectively. The response time to ethanol gas for undoped ZnO and Co- ZnO is ~2 and ~1 min at 300°C, respectively. In addition, the response time to acetone gas for undoped ZnO and Mn- ZnO is ~2 and ~3 min at 300°C, respectively.

Table 2: Response and recovery times of ZnO, Mn-ZnO and Co-ZnO sensors for different gases at 300°C.

Gas	Sample	T=300 °C	
		Response time(s)	Recovery time(min)
CO	ZnO	50	4
	Mn-ZnO	40	5
	Co-ZnO	200	8
Ethanol	ZnO	100	35
	Mn-ZnO	200	8
	Co-ZnO	50	5
Acetone	ZnO	120	5
	Mn-ZnO	200	7
	Co-ZnO	140	12

In n-type oxide semiconductors such as ZnO, the sensing response interaction to reducing gas involves in-diffusion of target gas onto the sensing body surface and subsequently oxidation by negative charged adsorbed oxygens, i.e. O^-or O^{2-}.[22] The rapid response of the sensors indicates that the diffusion and its oxidation with O^-or O^{2-} occur very speedily. Response time is depends on grain size and the size of the particle boundary in the material. [23] The smaller size of particles, the slower response time due to more diffusion of gas molecules. For Co-ZnO, the rapid response to ethanol than undoped ZnO is due to smaller crystallite size. While, Mn-ZnO with smallest crystallite size show slower response than undoped ZnO. In some sensors, high responses imply slow response times. Covalent bonding in sensitive materials reduces sensitivity and increase response times of these gas sensors.[23] On the other hand, the recovery times values of ZnO and Co-ZnO at 300°C sensors to 300 ppm ethanol are 35 and 5 min, respectively. The too long recovery times, particularly for ZnO sensor at 300°C can be attributed the inert surface adsorption, dissociation, and ionization of oxygen at the relatively low sensing temperatures.[24] Fig.9 shows response transients of the Co- ZnO sensor at 200°C -400°C for 300 ppm ethanol gas.

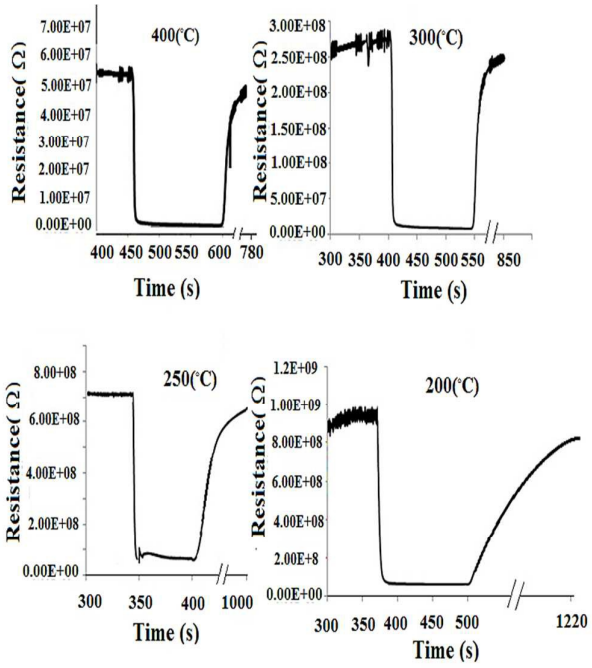

Fig. 9: Response transients of the Co- ZnO sensor at 200-400°C for 300 ppm ethanol gas.

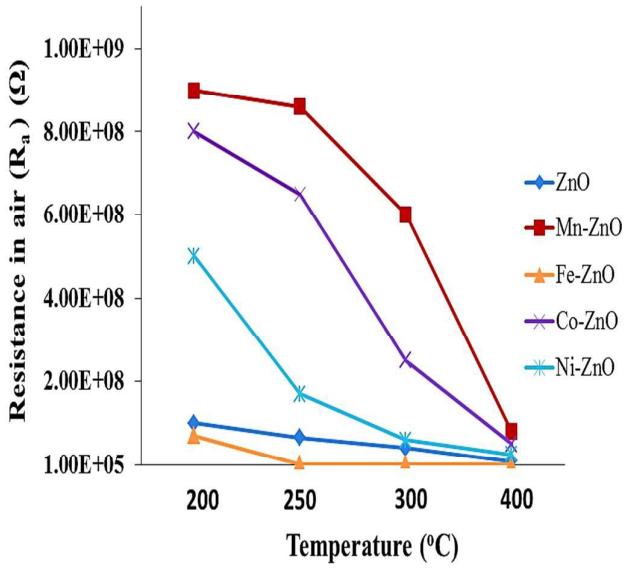

Fig.10. Resistances of the sensors in air as a function of temperature.

3.3.4 Resistance change of the sensors with temperature and dopants

Fig.10 shows resistances of the sensors in air at 200°C - 400°C as a function of temperature. As shown in this figure it is clear that resistance decreases as the temperature increases showing the semiconducting behavior of ZnO. The additions of dopants result in an extensive increase in the value of R_{air}, except Fe dopant. At doped ZnO with Co, Mn and Ni, the disorder produces in the lattice of ZnO due to difference in the ionic radii of Zn^{2+} and these ions. This disorder increases the efficiency of scattering mechanism such as phonon scattering and ionized impurity scattering which, in turn, causes an increase in resistivity. [25]

On the other hand, the doping of the ZnO by these donor dopants creates electronic defects in the same way that Al doped ZnO does [26], which causes the variations in the adsorbed oxygen. This develops a potential barrier which enhances the resistance of the material. [27]

The increase in resistivity is related to the strong oxygen adsorption on the doped ZnO surface at lower temperature such as 200°C. With increasing the temperature, the resistivity decreases, probably due to the dominant thermal excitation of electrons and the desorption of oxygen species. [25] While, in Fe -ZnO, the resistivity reduces in compared with undoped ZnO. It has been reported in some previous studies [28], when, Fe ions are substituted with Zn^{2+} ions in the tetrahedral sites of the wurtzite

structure of ZnO, valence state of Fe in ZnO is both +2 and +3, namely Fe in the ZnO matrix exists in a mixed valence state. Probably, the presence of Fe^{3+} ions in Fe-ZnO sample are expected to give rise to donor defects, thereby making the sample more conducting. [29]

3.3.5 Gas sensing mechanism

The difference in gas sensing property of undoped and doped ZnO for ethanol, acetone and CO gases can be explained by considering their sensing mechanism. A schematic presentation of sensing mechanism is shown in Figure 11. Gas sensing of ZnO sensors is based on the resistance change due to the chemical and electronic interaction between the gas and the ZnO. [30]

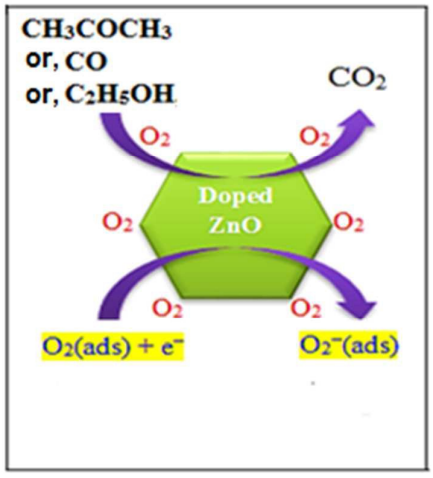

Fig.11: Schematic diagram of gas sensing mechanism.

When ZnO sensor is exposed to air, oxygen molecules adsorb on the surface of the materials to form O_2^-, O^-, O_2^- ions by capturing electrons from the conduction band. This leads to the formation of a thick space-charge layer which increases the potential barrier, and therefore, results in a higher resistance.

When the sensor of ZnO is exposed in CO, ethanol and acetone the adsorbed gas then reacts with the chemisorbed oxygen anions of surface, the reaction can be described as follows:

$$CO + O^- \rightarrow CO_2 + e^- \quad (1)$$

$$CH_3CH_2OH(ads) + 6O^-(ads) \rightarrow 2CO_2(g) + 3H_2O(l) + 6e^- \quad (2)$$

$$CH_3COCH_3(ads) + 8O^-(ads) \rightarrow 3CO_2(gas) + 3H_2O(gas) + 8e \quad (3)$$

The gas molecules will react with the adsorbed O^- to form CO_2 and H_2O, and release the trapped electrons back to the conduction band. The released electrons will reduce the thickness of the depletion region, and decrease the resistance of the ZnO. The doping of the ZnO by Co, Ni and Mn creates electronic defects and also changes the surface morphology of the films which causes the variations in the adsorbed oxygen. This develops a potential barrier which enhances the resistance of the material.[26]When doped ZnO is exposed to the gas (ethanol, acetone or CO), the chemisorbed oxygen will react with gas molecules due to the sensing reaction and re-inject the free carriers, thereby the resistance of the ZnO and doped ZnO reduce. The observed variations in the response of ZnO films at various dopants can be attributed to the variations in the electronic defects created due to

the different doping and to the variations in the adsorbed oxygen quantity.[31-33]

In addition, the gas sensing performance of ZnO is also greatly found to be dependent on the surface morphology.[34]

Recent studies reveal the surface structures and composition to be the essential factors governing the efficiency of gas sensing properties. They demonstrated that the enhancement in sensitivity of ZnO is attributed to the surface polarities of the different structures on the nanoscale. [35-37]

The polar [0001] and the [000$\bar{1}$] surfaces are among the most common crystal orientations of ZnO, which are capable of seizing atmospheric oxygen (O_2) through physical/chemical absorption due to unsaturated oxygen coordination. So, the (0001) facet has the highest chemisorption ability. The easy hydroxylation of this surface causes a metallization of the surface which can affect the conductivity response of such samples.[34] Most of the exposed surfaces of undoped ZnO, Mn-ZnO and Co-ZnO with hexagonal plate morphology are the Zn-terminated (0001) facets, and accordingly their performances as a ethanol gas sensor are significantly enhanced than the Ni-ZnO sensor with rod morphology.

In addition, the used dopants can significantly affect the sensing behavior of our gas sensors especially selectivity. These small dopant particles are located on the surface of a much bigger grain of zinc oxide that their distribution is assumed to be more or less homogenous.[21] According to spillover or catalytic effect model [21], the dopants that can act as catalyst, facilitates the activation of certain gas particles and reactions can be accelerated and influence on conductance if reaction take place on sensitive oxide surface. If a given catalyst facilitates the activation for only a definite gas, a higher selectivity can be obtained as we can observe in our sensors.

4. Conclusion

In summary, ZnO and dopeds ZnO nanostructures were prepared through asimple hydrothermal method. Systematical investigation on the effect of dopants on the sensing property of the host ZnO crystals was presented. The results displayed that the use of dopants affects structural, morphological, photoluminescence (PL), and sensing properties of ZnO. Co doped ZnO and undoped ZnO were selective sensors to ethanol and Ni- ZnO and Mn-ZnO were selective to acetone. While, Fe-ZnO did not show considerable response to that gases.

Acknowledgement

This work was supported by the Research Council of Shahid Rajaee Teacher Training University.

References

1. P. T. Mosely, B. C. Tofield, Solid State Gas Sensor, Adam Hilger, Bristol and Philadelphia, 1987.
2. L. Schmidt-Mende, J.L. Mac Manus-Driscoll, Mater. Today 2007, **10,** 40–48.
3. D. Calestani, M. Zha, R. Mosca, A. Zappettini, M.C. Carotta, V.D. Natale, L. Zanotti, Sens. Actuators B 2010, **144**,472–478.
4. M.J.S. Spencer, I. Yarovsky, J. Phys. Chem. C ,2010, **114**,10881–10893.
5. W.T. Moon, Y.K. Jun, H.S. Kim, W.S. Kim, S.H. Hong, J. Electro ceram, 2009, **23**,196–199.
6. Q. Wan, Q.H. Li, Y.J. Chen, T.H. Wang, X.L. He, J.P. Li, C.L. Lin, Appl. Phys. Lett, 2004**,84**,3654–3656.
7. J. Li, H.Q. Fan, X.H. Jia, J. Phys. Chem. C, 2010, **114**,14684–14691.
8. S.C. Navale, V. Ravi, I.S. Mulla, Sens. Actuators B, 2009, **139**,466–470.
9. X. Niu, W. Du, W. Du, Sens. Actuators B, 2004, **99**,405–409.
10. Y. Zeng, T. Zhang, L.J. Wang, M.H. Kang, H.T. Fan, R. Wang, Y. He, Sens. Actuators B: Chem, 2009, **140**,73–78.
11. N. Hana, , L. Chaia, , Q. Wang, Y. Tiana, P. Deng, Y. Chen, Sens. Actuators B: Chem, 2010**,147**, 525–530.
12. N. Faal Hamedani, A. R. Mahjoub, A. A. khodadadi, Y. Mortazavi, Sens. Actuators B: Chem, 2012, **169**,67– 73.
13. R.D. Shannon, Acta Cryst. A, 1976, **32**,751–767.
14. L. Yanmei, W. Tao, S. Xia, F. Qingqing, L. Qingrong, S. Xueping, S. Zaoqi, Appl Surf Sci, 2011,**257**, 6540–6545.
15. D. Wu, M. Yanga, Z. Huang, G. Yin, X. Liao, Y. Kang, X. Chen, H. Wang, Journal of Colloid and Interface Science, 2009, **330,**380–385.
16. K. Samanta, P. Bhattacharya, R. Katiyar, J. Appl. Phys, 2009, **105,**113929.
17. A.B. Djurisic, Y.H. Leung, K.H. Tam, Y.F. H.su, L.Ding, W.K. Ge, Y.C. Zhong, K.S. Wong, W.K. Chan, H.L. Tam, K.W. Cheah, W.M.K.wok, D.L. Phillips, 2007,**18**, 095702.
18. Y.Jin, Q. Cui, K. Wang, J. Hao, Q. Wang, J. Zhang, Journal of Applied Physics, 2011,**109,** 053521.
19. C. Karunakaran, J. Jayabharathi, K. Jayamoorthy, P. Vinayagamoorthy, Journal of Photochemistry and Photobiology A: Chemistry, 2012, **247**, 16–23.
20. C. Wang , L. Yin, L. Zhang, D. Xiang, R. Gao, Sensors 2010,**10,** 2088-2106.
21. P. Rai, R. Khan, R. Ahmad, Yoon-Bong Hahn, In-Hwan Lee, Yeon-Tae Yu, Current Applied Physics, 2013, **13**,1769-1773.
22. Z. Dai, L. Xu, G. Duan, T. Li, H. Zhang, Y. Li, Y. Wang, Y. Wang,W. Cai, Scientific Reports, 2013,**3**, 1669.

23. R. Vargas-Bernal, G. Herrera-Pérez, Nanotechnology for optics and sensors, 2014, 1-34.
24. Y. Zhang, J.Q. Xu, Q. Xiang, H. Li, Q.Y. Pan, P.C. Xu, J.Phys. Chem. C, 2009, **113,**3430–3435.
25. P.P. Sahay, R.K. Nath, Al-doped ZnO thin films as methanol sensors, Sens. Actuators B: Chem, 2008,**134**, 654–659.
26. K.F. Cai, E. Müller, C. Draˇsar, A. Mrotzek, Mater. Sci. Eng. B, 2003,**104**, 45–48.
27. T. T. Trinh, N. H. Tu, H. H. Le, K. Y. Ryu, K. B. Le, K. Pillai, J. Yi, , Sens. Actuators B: Chem, 2011, **152,**73–81.
28. M. S. Shubra Singh, R. Ramachandra, Phsical Review B, 2009, **80**,045210.
29. H. Colak, O. Turkoglu, Synthesis, J. Mater. Sci. Technol., 2012, **28**,268-274.
30. P. Rai, Y-T. Yu, Sens. Actuators B: Chem, 2012,**173**, 58–65.
31. H. Gu, Z. Wang, Y. Hu, Hydrogen Gas Sensors, 2012, **12,**5517-5550.
32. S. M. Chou, L. G. Teoh, W. H. Lai, Y. H. Su, M. H. Hon, Sensors (Basel), 2006,**6**,1420–1427.
33. N. Singh, C. Yan, P. S. Lee, Sens. Actuators B: Chem, 2010, **150,**19–24.
34. R. Kumar, O. Al-Dossary, G. Kumar, A. Umar, Nano-Micro Lett, 2015, **7(2)**, 97–120.
35. N. Han, X. Wu, L. Chai, H. Liu, Y. Chen, Sens. Actuators B: Chem, 2010,**150(1),** 230–238.
36. M. R. Alenezi, A. S. Alshammari, K. D. G. I. Jayawardena, M. J Beliatis, S. J. Henley, S. R. P. Silva, J. Phys. Chem. C, 2013, **117**,17850−17858.
37. Y. V. Kaneti , Z. Zhang , J. Yue , Q. M. Zakaria , C. Chen , X. Jiang , A. Yu , Phys Chem Chem Phys. 2014, **16(23)**, 11471-80.